FERMILAB-PUB-12-650-E

Measurement of the combined rapidity and p_T dependence of dijet azimuthal decorrelations in $p\bar{p}$ collisions at $\sqrt{s} = 1.96\,\text{TeV}$

V.M. Abazov,[32] B. Abbott,[68] B.S. Acharya,[26] M. Adams,[46] T. Adams,[44] G.D. Alexeev,[32] G. Alkhazov,[36] A. Alton[a],[57] A. Askew,[44] S. Atkins,[55] K. Augsten,[7] C. Avila,[5] F. Badaud,[10] L. Bagby,[45] B. Baldin,[45] D.V. Bandurin,[44] S. Banerjee,[26] E. Barberis,[56] P. Baringer,[53] J.F. Bartlett,[45] U. Bassler,[15] V. Bazterra,[46] A. Bean,[53] M. Begalli,[2] L. Bellantoni,[45] S.B. Beri,[24] G. Bernardi,[14] R. Bernhard,[19] I. Bertram,[39] M. Besançon,[15] R. Beuselinck,[40] P.C. Bhat,[45] S. Bhatia,[59] V. Bhatnagar,[24] G. Blazey,[47] S. Blessing,[44] K. Bloom,[60] A. Boehnlein,[45] D. Boline,[65] E.E. Boos,[34] G. Borissov,[39] A. Brandt,[71] O. Brandt,[20] R. Brock,[58] A. Bross,[45] D. Brown,[14] J. Brown,[14] X.B. Bu,[45] M. Buehler,[45] V. Buescher,[21] V. Bunichev,[34] S. Burdin[b],[39] C.P. Buszello,[38] E. Camacho-Pérez,[29] B.C.K. Casey,[45] H. Castilla-Valdez,[29] S. Caughron,[58] S. Chakrabarti,[65] D. Chakraborty,[47] K. Chakravarthula,[55] K.M. Chan,[51] A. Chandra,[73] E. Chapon,[15] G. Chen,[53] S.W. Cho,[28] S. Choi,[28] B. Choudhary,[25] S. Cihangir,[45] D. Claes,[60] J. Clutter,[53] M. Cooke,[45] W.E. Cooper,[45] M. Corcoran,[73] F. Couderc,[15] M.-C. Cousinou,[12] D. Cutts,[70] A. Das,[42] G. Davies,[40] S.J. de Jong,[30,31] E. De La Cruz-Burelo,[29] F. Déliot,[15] R. Demina,[64] D. Denisov,[45] S.P. Denisov,[35] S. Desai,[45] C. Deterre[d],[20] K. DeVaughan,[60] H.T. Diehl,[45] M. Diesburg,[45] P.F. Ding,[41] A. Dominguez,[60] A. Dubey,[25] L.V. Dudko,[34] D. Duggan,[61] A. Duperrin,[12] S. Dutt,[24] A. Dyshkant,[47] M. Eads,[47] D. Edmunds,[58] J. Ellison,[43] V.D. Elvira,[45] Y. Enari,[14] H. Evans,[49] V.N. Evdokimov,[35] G. Facini,[56] L. Feng,[47] T. Ferbel,[64] F. Fiedler,[21] F. Filthaut,[30,31] W. Fisher,[58] H.E. Fisk,[45] M. Fortner,[47] H. Fox,[39] S. Fuess,[45] A. Garcia-Bellido,[64] J.A. García-González,[29] G.A. García-Guerra[c],[29] V. Gavrilov,[33] W. Geng,[12,58] C.E. Gerber,[46] Y. Gershtein,[61] G. Ginther,[45,64] G. Golovanov,[32] P.D. Grannis,[65] S. Greder,[16] H. Greenlee,[45] G. Grenier,[17] Ph. Gris,[10] J.-F. Grivaz,[13] A. Grohsjean[d],[15] S. Grünendahl,[45] M.W. Grünewald,[27] T. Guillemin,[13] G. Gutierrez,[45] P. Gutierrez,[68] J. Haley,[56] L. Han,[4] K. Harder,[41] A. Harel,[64] J.M. Hauptman,[52] J. Hays,[40] T. Head,[41] T. Hebbeker,[18] D. Hedin,[47] H. Hegab,[69] A.P. Heinson,[43] U. Heintz,[70] C. Hensel,[20] I. Heredia-De La Cruz,[29] K. Herner,[57] G. Hesketh[f],[41] M.D. Hildreth,[51] R. Hirosky,[74] T. Hoang,[44] J.D. Hobbs,[65] B. Hoeneisen,[9] J. Hogan,[73] M. Hohlfeld,[21] I. Howley,[71] Z. Hubacek,[7,15] V. Hynek,[7] I. Iashvili,[63] Y. Ilchenko,[72] R. Illingworth,[45] A.S. Ito,[45] S. Jabeen,[70] M. Jaffré,[13] A. Jayasinghe,[68] M.S. Jeong,[28] R. Jesik,[40] P. Jiang,[4] K. Johns,[42] E. Johnson,[58] M. Johnson,[45] A. Jonckheere,[45] P. Jonsson,[40] J. Joshi,[43] A.W. Jung,[45] A. Juste,[37] E. Kajfasz,[12] D. Karmanov,[34] P.A. Kasper,[45] I. Katsanos,[60] R. Kehoe,[72] S. Kermiche,[12] N. Khalatyan,[45] A. Khanov,[69] A. Kharchilava,[63] Y.N. Kharzheev,[32] I. Kiselevich,[33] J.M. Kohli,[24] A.V. Kozelov,[35] J. Kraus,[59] A. Kumar,[63] A. Kupco,[8] T. Kurča,[17] V.A. Kuzmin,[34] S. Lammers,[49] G. Landsberg,[70] P. Lebrun,[17] H.S. Lee,[28] S.W. Lee,[52] W.M. Lee,[44] X. Lei,[42] J. Lellouch,[14] D. Li,[14] H. Li,[74] L. Li,[43] Q.Z. Li,[45] J.K. Lim,[28] D. Lincoln,[45] J. Linnemann,[58] V.V. Lipaev,[35] R. Lipton,[45] H. Liu,[72] Y. Liu,[4] A. Lobodenko,[36] M. Lokajicek,[8] R. Lopes de Sa,[65] R. Luna-Garcia[g],[29] A.L. Lyon,[45] A.K.A. Maciel,[1] R. Magaña-Villalba,[29] S. Malik,[60] V.L. Malyshev,[32] Y. Maravin,[54] J. Martínez-Ortega,[29] R. McCarthy,[65] C.L. McGivern,[41] M.M. Meijer,[30,31] A. Melnitchouk,[45] D. Menezes,[47] P.G. Mercadante,[3] M. Merkin,[34] A. Meyer,[18] J. Meyer,[20] F. Miconi,[16] N.K. Mondal,[26] M. Mulhearn,[74] E. Nagy,[12] M. Naimuddin,[25] M. Narain,[70] R. Nayyar,[42] H.A. Neal,[57] J.P. Negret,[5] P. Neustroev,[36] H.T. Nguyen,[74] T. Nunnemann,[22] J. Orduna,[73] N. Osman,[12] J. Osta,[51] M. Padilla,[43] A. Pal,[71] N. Parashar,[50] V. Parihar,[70] S.K. Park,[28] R. Partridge[e],[70] N. Parua,[49] A. Patwa,[66] B. Penning,[45] M. Perfilov,[34] Y. Peters,[20] K. Petridis,[41] G. Petrillo,[64] P. Pétroff,[13] M.-A. Pleier,[66] P.L.M. Podesta-Lerma[h],[29] V.M. Podstavkov,[45] A.V. Popov,[35] M. Prewitt,[73] D. Price,[49] N. Prokopenko,[35] J. Qian,[57] A. Quadt,[20] B. Quinn,[59] M.S. Rangel,[1] K. Ranjan,[25] P.N. Ratoff,[39] I. Razumov,[35] P. Renkel,[72] I. Ripp-Baudot,[16] F. Rizatdinova,[69] M. Rominsky,[45] A. Ross,[39] C. Royon,[15] P. Rubinov,[45] R. Ruchti,[51] G. Sajot,[11] P. Salcido,[47] A. Sánchez-Hernández,[29] M.P. Sanders,[22] A.S. Santos[i],[1] G. Savage,[45] L. Sawyer,[55] T. Scanlon,[40] R.D. Schamberger,[65] Y. Scheglov,[36] H. Schellman,[48] C. Schwanenberger,[41] R. Schwienhorst,[58] J. Sekaric,[53] H. Severini,[68] E. Shabalina,[20] V. Shary,[15] S. Shaw,[58] A.A. Shchukin,[35] R.K. Shivpuri,[25] V. Simak,[7] P. Skubic,[68] P. Slattery,[64] D. Smirnov,[51] K.J. Smith,[63] G.R. Snow,[60] J. Snow,[67] S. Snyder,[66] S. Söldner-Rembold,[41] L. Sonnenschein,[18] K. Soustruznik,[6] J. Stark,[11] D.A. Stoyanova,[35] M. Strauss,[68] L. Suter,[41] P. Svoisky,[68] M. Titov,[15] V.V. Tokmenin,[32] Y.-T. Tsai,[64] D. Tsybychev,[65] B. Tuchming,[15] C. Tully,[62] L. Uvarov,[36] S. Uvarov,[36] S. Uzunyan,[47] R. Van Kooten,[49] W.M. van Leeuwen,[30] N. Varelas,[46] E.W. Varnes,[42] I.A. Vasilyev,[35] P. Verdier,[17] A.Y. Verkheev,[32] L.S. Vertogradov,[32] M. Verzocchi,[45] M. Vesterinen,[41] D. Vilanova,[15] P. Vokac,[7] H.D. Wahl,[44]

M.H.L.S. Wang,[45] J. Warchol,[51] G. Watts,[75] M. Wayne,[51] J. Weichert,[21] L. Welty-Rieger,[48] A. White,[71] D. Wicke,[23] M.R.J. Williams,[39] G.W. Wilson,[53] M. Wobisch,[55] D.R. Wood,[56] T.R. Wyatt,[41] Y. Xie,[45] R. Yamada,[45] S. Yang,[4] T. Yasuda,[45] Y.A. Yatsunenko,[32] W. Ye,[65] Z. Ye,[45] H. Yin,[45] K. Yip,[66] S.W. Youn,[45] J.M. Yu,[57] J. Zennamo,[63] T.G. Zhao,[41] B. Zhou,[57] J. Zhu,[57] M. Zielinski,[64] D. Zieminska,[49] and L. Zivkovic[14]

(The D0 Collaboration*)

[1]*LAFEX, Centro Brasileiro de Pesquisas Físicas, Rio de Janeiro, Brazil*
[2]*Universidade do Estado do Rio de Janeiro, Rio de Janeiro, Brazil*
[3]*Universidade Federal do ABC, Santo André, Brazil*
[4]*University of Science and Technology of China, Hefei, People's Republic of China*
[5]*Universidad de los Andes, Bogotá, Colombia*
[6]*Charles University, Faculty of Mathematics and Physics, Center for Particle Physics, Prague, Czech Republic*
[7]*Czech Technical University in Prague, Prague, Czech Republic*
[8]*Center for Particle Physics, Institute of Physics, Academy of Sciences of the Czech Republic, Prague, Czech Republic*
[9]*Universidad San Francisco de Quito, Quito, Ecuador*
[10]*LPC, Université Blaise Pascal, CNRS/IN2P3, Clermont, France*
[11]*LPSC, Université Joseph Fourier Grenoble 1, CNRS/IN2P3, Institut National Polytechnique de Grenoble, Grenoble, France*
[12]*CPPM, Aix-Marseille Université, CNRS/IN2P3, Marseille, France*
[13]*LAL, Université Paris-Sud, CNRS/IN2P3, Orsay, France*
[14]*LPNHE, Universités Paris VI and VII, CNRS/IN2P3, Paris, France*
[15]*CEA, Irfu, SPP, Saclay, France*
[16]*IPHC, Université de Strasbourg, CNRS/IN2P3, Strasbourg, France*
[17]*IPNL, Université Lyon 1, CNRS/IN2P3, Villeurbanne, France and Université de Lyon, Lyon, France*
[18]*III. Physikalisches Institut A, RWTH Aachen University, Aachen, Germany*
[19]*Physikalisches Institut, Universität Freiburg, Freiburg, Germany*
[20]*II. Physikalisches Institut, Georg-August-Universität Göttingen, Göttingen, Germany*
[21]*Institut für Physik, Universität Mainz, Mainz, Germany*
[22]*Ludwig-Maximilians-Universität München, München, Germany*
[23]*Fachbereich Physik, Bergische Universität Wuppertal, Wuppertal, Germany*
[24]*Panjab University, Chandigarh, India*
[25]*Delhi University, Delhi, India*
[26]*Tata Institute of Fundamental Research, Mumbai, India*
[27]*University College Dublin, Dublin, Ireland*
[28]*Korea Detector Laboratory, Korea University, Seoul, Korea*
[29]*CINVESTAV, Mexico City, Mexico*
[30]*Nikhef, Science Park, Amsterdam, the Netherlands*
[31]*Radboud University Nijmegen, Nijmegen, the Netherlands*
[32]*Joint Institute for Nuclear Research, Dubna, Russia*
[33]*Institute for Theoretical and Experimental Physics, Moscow, Russia*
[34]*Moscow State University, Moscow, Russia*
[35]*Institute for High Energy Physics, Protvino, Russia*
[36]*Petersburg Nuclear Physics Institute, St. Petersburg, Russia*
[37]*Institució Catalana de Recerca i Estudis Avançats (ICREA) and Institut de Física d'Altes Energies (IFAE), Barcelona, Spain*
[38]*Uppsala University, Uppsala, Sweden*
[39]*Lancaster University, Lancaster LA1 4YB, United Kingdom*
[40]*Imperial College London, London SW7 2AZ, United Kingdom*
[41]*The University of Manchester, Manchester M13 9PL, United Kingdom*
[42]*University of Arizona, Tucson, Arizona 85721, USA*
[43]*University of California Riverside, Riverside, California 92521, USA*
[44]*Florida State University, Tallahassee, Florida 32306, USA*
[45]*Fermi National Accelerator Laboratory, Batavia, Illinois 60510, USA*
[46]*University of Illinois at Chicago, Chicago, Illinois 60607, USA*
[47]*Northern Illinois University, DeKalb, Illinois 60115, USA*
[48]*Northwestern University, Evanston, Illinois 60208, USA*
[49]*Indiana University, Bloomington, Indiana 47405, USA*
[50]*Purdue University Calumet, Hammond, Indiana 46323, USA*
[51]*University of Notre Dame, Notre Dame, Indiana 46556, USA*
[52]*Iowa State University, Ames, Iowa 50011, USA*
[53]*University of Kansas, Lawrence, Kansas 66045, USA*
[54]*Kansas State University, Manhattan, Kansas 66506, USA*

[55]Louisiana Tech University, Ruston, Louisiana 71272, USA
[56]Northeastern University, Boston, Massachusetts 02115, USA
[57]University of Michigan, Ann Arbor, Michigan 48109, USA
[58]Michigan State University, East Lansing, Michigan 48824, USA
[59]University of Mississippi, University, Mississippi 38677, USA
[60]University of Nebraska, Lincoln, Nebraska 68588, USA
[61]Rutgers University, Piscataway, New Jersey 08855, USA
[62]Princeton University, Princeton, New Jersey 08544, USA
[63]State University of New York, Buffalo, New York 14260, USA
[64]University of Rochester, Rochester, New York 14627, USA
[65]State University of New York, Stony Brook, New York 11794, USA
[66]Brookhaven National Laboratory, Upton, New York 11973, USA
[67]Langston University, Langston, Oklahoma 73050, USA
[68]University of Oklahoma, Norman, Oklahoma 73019, USA
[69]Oklahoma State University, Stillwater, Oklahoma 74078, USA
[70]Brown University, Providence, Rhode Island 02912, USA
[71]University of Texas, Arlington, Texas 76019, USA
[72]Southern Methodist University, Dallas, Texas 75275, USA
[73]Rice University, Houston, Texas 77005, USA
[74]University of Virginia, Charlottesville, Virginia 22904, USA
[75]University of Washington, Seattle, Washington 98195, USA

(Dated: December 8, 2012)

We present the first combined measurement of the rapidity and transverse momentum dependence of dijet azimuthal decorrelations, using the recently proposed quantity $R_{\Delta\phi}$. The variable $R_{\Delta\phi}$ measures the fraction of the inclusive dijet events in which the azimuthal separation of the two jets with the highest transverse momenta is less than a specified value for the parameter $\Delta\phi_{\rm max}$. The quantity $R_{\Delta\phi}$ is measured in $p\bar{p}$ collisions at $\sqrt{s} = 1.96\,\text{TeV}$, as a function of the dijet rapidity interval, the total scalar transverse momentum, and $\Delta\phi_{\rm max}$. The measurement uses an event sample corresponding to an integrated luminosity of $0.7\,\text{fb}^{-1}$ collected with the D0 detector at the Fermilab Tevatron Collider. The results are compared to predictions of a perturbative QCD calculation at next-to-leading order in the strong coupling with corrections for non-perturbative effects. The theory predictions describe the data, except in the kinematic region of large dijet rapidity intervals and large $\Delta\phi_{\rm max}$.

PACS numbers: 13.87.Ce, 12.38.Qk

In high-energy collisions of hadrons, the production rates of particle jets with large transverse momentum with respect to the beam direction, p_T, are predicted by perturbative Quantum Chromodynamics (pQCD). At second order in the strong coupling constant, α_s, pQCD predicts only the production of dijet final states. In the absence of higher-order radiative effects, the jet directions are correlated in the azimuthal plane and their relative azimuthal angle $\Delta\phi_{\rm dijet} = |\phi_{\rm jet1} - \phi_{\rm jet2}|$ is equal to π. Deviations from π (hereafter referred to as "azimuthal decorrelations") are caused by radiative processes in which additional jets are produced. The amount of the decorrelation is directly related to the multiplicity and the p_T carried by the additional jets. The transition from soft to hard higher-order pQCD processes can be studied by examining the corresponding range of azimuthal decorrelations from small to large values. This makes measurements of dijet azimuthal decorrelations an ideal testing ground for pQCD predictions of multijet production processes. In pQCD, dijet azimuthal decorrelations are predicted to depend not only on the transverse momentum of the jets, but also on the rapidity $y^* = |y_{\rm jet1} - y_{\rm jet2}|/2$, obtained from the rapidity difference of the two leading p_T jets in an event [1]. In a previous analysis of dijet azimuthal decorrelations, we measured the dijet differential cross section as a function of $\Delta\phi_{\rm dijet}$, integrated over a fixed jet rapidity range and normalized by the inclusive dijet cross section, for different requirements on the leading jet p_T [2]. The same methodology was later used in analyses of pp collision data at $\sqrt{s} = 7\,\text{TeV}$ from the CERN Large Hadron Collider [3, 4]. In all cases, dijet azimuthal decorrelations have been observed to decrease with increasing p_T; however, the combined rapidity and p_T dependence has not yet been measured.

In this Letter, we perform a measurement of the rapidity and the p_T dependence of dijet azimuthal decor-

*with visitors from [a]Augustana College, Sioux Falls, SD, USA, [b]The University of Liverpool, Liverpool, UK, [c]UPIITA-IPN, Mexico City, Mexico, [d]DESY, Hamburg, Germany, [e]SLAC, Menlo Park, CA, USA, [f]University College London, London, UK, [g]Centro de Investigacion en Computacion - IPN, Mexico City, Mexico, [h]ECFM, Universidad Autonoma de Sinaloa, Culiacán, Mexico and [i]Universidade Estadual Paulista, São Paulo, Brazil.

relations. The analysis is based on a new quantity, $R_{\Delta\phi}$, which was recently proposed in Ref. [5] as

$$R_{\Delta\phi}(H_T, y^*, \Delta\phi_{\rm max}) = \frac{\frac{d^2\sigma_{\rm dijet}(\Delta\phi_{\rm dijet}<\Delta\phi_{\rm max})}{dH_T\,dy^*}}{\frac{d^2\sigma_{\rm dijet}({\rm inclusive})}{dH_T\,dy^*}}. \quad (1)$$

The quantity $R_{\Delta\phi}$ is defined as the fraction of the inclusive dijet cross section with a decorrelation of $\Delta\phi_{\rm dijet} < \Delta\phi_{\rm max}$, where $\Delta\phi_{\rm max}$ is a parameter and $\sigma_{\rm dijet}({\rm inclusive})$ is the inclusive dijet cross section without a $\Delta\phi_{\rm dijet}$ requirement. It is measured as a function of $\Delta\phi_{\rm max}$, y^*, and of the total transverse momentum H_T in the event, computed as the scalar p_T sum from all jets i with $p_{Ti} > p_{T\rm min}$ and $|y_i - y_{\rm boost}| < y^*_{\rm max}$ where $y_{\rm boost} = (y_{\rm jet1} + y_{\rm jet2})/2$, $p_{T\rm min} = 30\,{\rm GeV}$, and $y^*_{\rm max} = 2$, where jet1 and jet2 are the jets with the largest p_T in the event. For $\Delta\phi_{\rm max} \approx \pi$, $R_{\Delta\phi}$ is sensitive to soft QCD radiation, while it becomes sensitive to hard higher-order QCD processes for smaller values of $\Delta\phi_{\rm max}$. The phase space region $\Delta\phi_{\rm max} < 2\pi/3$ is dominated by final states with four or more jets. Since $R_{\Delta\phi}$ is defined as a ratio of cross sections, several experimental and theoretical uncertainties cancel. In pQCD, $R_{\Delta\phi}$ is computed as a ratio of three-jet and dijet cross sections which is (at leading order, LO) proportional to α_s. While dependencies on parton distribution functions (PDFs) largely cancel, $R_{\Delta\phi}$ is sensitive to the pQCD matrix elements and to α_s.

The measurement is performed in $p\bar{p}$ collisions at $\sqrt{s} = 1.96\,{\rm TeV}$, for an inclusive dijet event sample defined by the Run II midpoint cone jet algorithm [6] with a cone of radius $R_{\rm cone} = 0.7$ in y and ϕ. The dijet phase space is defined by the requirements $p_{T1} > H_T/3$, $p_{T2} > p_{T\rm min}$, $y^* < y^*_{\rm max}$, and $|y_{\rm boost}| < 0.5$. Following the proposal in Ref. [5], $R_{\Delta\phi}$ is measured over the H_T range of 180–900 GeV, in three rapidity regions of $0 < y^* < 0.5$, $0.5 < y^* < 1$, and $1 < y^* < 2$; and for $\Delta\phi_{\rm max} = 7\pi/8$, $5\pi/6$, and $3\pi/4$. The ranges in y^* and $y_{\rm boost}$, and the value of $p_{T\rm min}$ ensure that all jets are always within $|y| < 2.5$ at p_T values where the jet energy calibration and jet p_T resolutions are known with high precision. The requirement $p_{T1} > H_T/3$ provides a lower boundary for the leading jet p_T in each H_T bin, which (together with $|y| < 2.5$) ensures that the jet triggers are efficient. The data are corrected for experimental effects and are presented at the "particle level," which includes all stable particles as defined in Ref. [7].

A detailed description of the D0 detector is provided in Ref. [8]. The event triggering and selection, jet reconstruction, and jet energy and momentum correction are identical to those used in recent D0 multijet measurements [9–13]. Jets are reconstructed in the finely segmented liquid-argon sampling calorimeters that cover most of the solid angle. The central calorimeter covers polar angles in the range 37–143° and the two endcap calorimeters extend this coverage to within 1.7° of the nominal beamline [8]. The transition regions between the central and the endcap calorimeters contain scintillator-based detectors to improve the energy sampling. The jet transverse momenta are calculated using only calorimeter information and the location of the $p\bar{p}$ collision. The position of the $p\bar{p}$ interaction is determined from the tracks reconstructed based on data from the silicon detector and scintillating fiber tracker located inside a 2 T solenoidal magnet [8]. The position is required to be within 50 cm of the detector center in the coordinate along the beam axis, with at least three tracks pointing to it. These requirements discard (7–9)% of the events, depending on the trigger used. For this measurement, events are triggered by inclusive jet triggers. Trigger efficiencies are studied as a function of H_T by comparing the inclusive dijet cross section in data sets obtained by triggers with different p_T thresholds in regions where the trigger with lower threshold is fully efficient. The trigger with lowest p_T threshold is shown to be fully efficient by studying an event sample obtained independently with a muon trigger. In each inclusive jet H_T bin, events are used from a single trigger which has an efficiency higher than 98%. Requirements on the characteristics of the calorimeter clusters shower shapes are used to suppress the background due to electrons, photons, and detector noise that would otherwise mimic jets. The efficiency for the shower shape requirements is above 97.5%. Contributions from cosmic ray events are suppressed by requiring the missing transverse momentum in an event to be less than 70% (50%) of the leading jet p_T (before the jet energy calibration is applied) if the latter is below (above) 100 GeV. The efficiency of this requirement for signal is found to be > 99.5% [14, 15]. After all selection requirements, the fraction of background events is below 0.1% for all H_T, as determined from distributions in signal and in background-enriched event samples.

The jet four-momenta reconstructed from calorimeter energy depositions are then corrected, on average, for the response of the calorimeter, the net energy flow through the jet cone, additional energy from previous beam crossings, and multiple $p\bar{p}$ interactions in the same event, but not for the presence of muons and neutrinos [14, 15]. These corrections adjust the reconstructed jet energy to the energy of the stable particles that enter the calorimeter except for muons and neutrinos. The absolute energy calibration is determined from $Z \to e^+e^-$ events and the p_T imbalance in γ + jet events in the region $|y| < 0.4$. The extension to larger rapidities is derived from dijet events using a similar data-driven method. In addition, corrections in the range (2–4)% are applied that take into account the difference in calorimeter response due to the difference in the fractional contributions of quark and gluon-initiated jets in the dijet and the γ + jet event samples. These corrections are determined using jets simulated with the PYTHIA event generator [16] that have been passed through a GEANT-based detector simulation [17]. The total corrections of the jet four-momenta

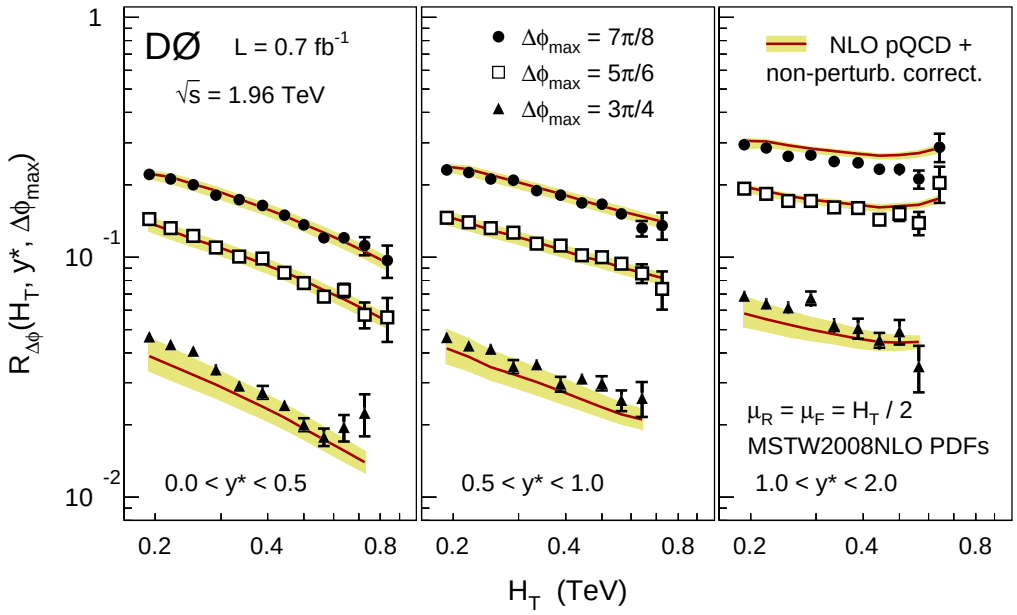

FIG. 1: (Color online.) The results for $R_{\Delta\phi}$ as a function of H_T in three different regions of y^* and for three different $\Delta\phi_{\rm max}$ requirements. The error bars indicate the statistical and systematic uncertainties summed in quadrature. The theoretical predictions are shown with their uncertainties.

vary between 50% and 20% for jet p_T between 50 and 400 GeV. An additional correction is applied for systematic shifts in rapidity due to detector effects [14, 15].

The procedure that corrects the distributions $R_{\Delta\phi}(H_T, y^*, \Delta\phi_{\rm max})$ for experimental effects uses particle-level events, generated with SHERPA 1.1.3 [18] with MSTW2008LO PDFs [19] and with PYTHIA 6.419 [16] with CTEQ6.6 PDFs [20] and tune QW [21]. The jets from these events are processed by a simulation of the detector response which is based on parametrizations of jet p_T resolutions and jet reconstruction efficiencies determined from data and of resolutions of the polar and azimuthal angles of jets, obtained from a detailed simulation of the detector using GEANT.

The p_T resolution for jets is about 15% at 40 GeV, decreasing to less than 10% at 400 GeV. To use the simulation to correct for experimental effects, the simulation must describe all relevant distributions, including the p_T and $|y|$ distributions of the three leading p_T jets, and the $\Delta\phi_{\rm dijet}$ distribution. To achieve this, the generated events, which are used in the correction procedure, are weighted, based on the properties of the generated jets, to match these distributions in data. The bin sizes in the H_T distributions are chosen to be approximately twice the H_T resolution. The bin purity, defined as the fraction of all reconstructed events that were generated in the same bin, is above 50% for all bins, and only weakly dependent on H_T. We then use the simulation to determine correction factors for experimental effects for all bins. The correction factors are computed bin-by-bin as the ratio of $R_{\Delta\phi}$ without and with simulation of the detector response. These also include corrections for the energies of unreconstructed muons and neutrinos inside the jets. The total correction factors for $R_{\Delta\phi}$ using the weighted PYTHIA and SHERPA simulations agree typically within 1% for $\Delta\phi_{\rm max} = 7\pi/8$ and $5\pi/6$ and between 1–4% for $\Delta\phi_{\rm max} = 3\pi/4$. The total correction factors, defined as the average values from PYTHIA and SHERPA, are 0.98–1.0 for $\Delta\phi_{\rm max} = 7\pi/8$, 0.95–0.99 for $\Delta\phi_{\rm max} = 5\pi/6$, and 0.81–0.91 for $\Delta\phi_{\rm max} = 3\pi/4$, with little y^* dependence. The difference between the average and the individual corrections is taken into account as the uncertainty attributed to the model dependence.

In total, 69 independent sources of experimental systematic uncertainties are identified, mostly related to jet energy calibration and jet p_T resolution. The effects of each source are taken as fully correlated between all data points. The dominant uncertainties for the $R_{\Delta\phi}$ distributions are due to the jet energy calibration (2–5)%, and the model dependence of the correction factors (1–4)%. Smaller contributions come from the jet ϕ resolution (0.5–2)%, from the uncertainties in systematic shifts in y ($< 2\%$), and the jet p_T resolution ($< 1\%$). All other sources are negligible. The systematic uncertainties are 2–3% for $\Delta\phi_{\rm max} = 7\pi/8$ and $5\pi/6$ and 3–5% for $\Delta\phi_{\rm max} = 3\pi/4$. A detailed documentation of the results, including the individual contributions to the uncertainties, is provided in the supplementary material [22].

The results for $R_{\Delta\phi}(H_T, y^*, \Delta\phi_{\rm max})$ are listed in Tables I–III and displayed in Fig. 1 as a function of H_T, in different regions of y^* and for different $\Delta\phi_{\rm max}$. A subset of the data points from selected H_T regions are

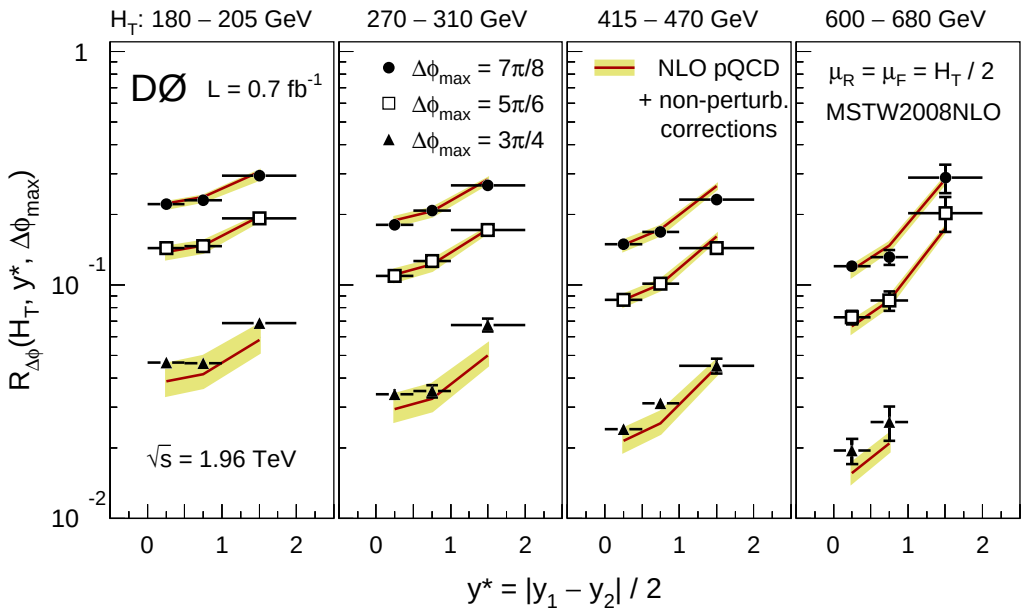

FIG. 2: (Color online.) The results for $R_{\Delta\phi}$ as a function of y^* in four different regions of H_T and for three different $\Delta\phi_{\rm max}$ requirements. The error bars indicate the statistical and systematic uncertainties summed in quadrature. The theoretical predictions are shown with their uncertainties.

also shown in Fig. 2, where $R_{\Delta\phi}$ is displayed as a function of y^* for different choices of $\Delta\phi_{\rm max}$. The values of H_T and y^* at which the data points are presented correspond to the arithmetic centers of the bins. Figure 1 shows that for all choices of $\Delta\phi_{\rm max}$ and in all y^* regions, $R_{\Delta\phi}$ decreases with H_T. In all y^* regions, the H_T dependence increases towards lower $\Delta\phi_{\rm max}$, and for all $\Delta\phi_{\rm max}$ requirements the H_T dependence becomes stronger for smaller y^*. This implies that the y^* dependence of $R_{\Delta\phi}$ increases with increasing H_T, as shown in Fig. 2.

The theoretical predictions for $R_{\Delta\phi}$ are obtained from a pQCD calculation in next-to-leading order (NLO), in α_s, with corrections for non-perturbative effects. The latter include contributions from hadronization and the underlying event. The non-perturbative corrections are determined using PYTHIA 6.426 with tunes AMBT1 [23] and DW [21] which use different parton shower and underlying event models. The hadronization correction is obtained from the ratio of $R_{\Delta\phi}$ on the parton level after the parton shower and the particle level including all stable particles, both without the underlying event. The underlying-event correction is computed from the ratio of $R_{\Delta\phi}$ computed at the particle level with and without underlying event. The total correction is given by the product of the two individual correction factors for hadronization and the underlying event. The total corrections vary between +1% and −1% for tune AMBT1 and between +1% and −3% for tune DW. The results obtained with the two tunes agree typically within 1% and always within 3% [5]. The central results are taken to be the average values, and the uncertainty is taken to be half of the difference. As a cross-check, the non-perturbative corrections are also derived with HERWIG 6.520 [24, 25], using default settings. The HERWIG and PYTHIA results agree typically within 0.5%, and always within 1% (3%) for $\Delta\phi_{\rm max} = 7\pi/8$ and $5\pi/6$ (for $\Delta\phi_{\rm max} = 3\pi/4$) [5].

The NLO (LO) pQCD prediction for $R_{\Delta\phi}$ is computed as the ratio of the NLO (LO) predictions for the numerator and the denominator. The NLO prediction for the numerator (denominator) is obtained from an $\mathcal{O}(\alpha_s^4)$ ($\mathcal{O}(\alpha_s^3)$) cross section calculation. These results are computed using FASTNLO [26, 27] based on NLOJET++ [28, 29], in the $\overline{\rm MS}$ scheme [30] for five active quark flavors. The calculations use the next-to-leading logarithmic (two-loop) approximation of the renormalization group equation and $\alpha_s(M_Z) = 0.118$ in the matrix elements and the PDFs, which is close to the current world average value of 0.1184 ± 0.0007 [31]. The MSTW2008NLO PDFs [19] are used, and the central choice μ_0 for the renormalization and factorization scales is $\mu_R = \mu_F = \mu_0 = H_T/2$, which is identical to $\mu_0 = p_T$ for inclusive jet and dijet production at LO. The theoretical predictions are overlaid on the data in Figs. 1 and 2, and some properties are displayed in Fig. 3. The PDF uncertainties are computed using the up and down variations of the 20 orthogonal PDF uncertainty eigenvectors, corresponding to the 68% C.L., as provided by MSTW2008NLO. The PDF uncertainties are typically 1%, and never larger than 2%. The $R_{\Delta\phi}$ results obtained with the CT10 [32] and NNPDFv2.1 [33] PDF parametrizations agree with those for MSTW2008NLO within 2%. The theoretical uncertainties are dominated

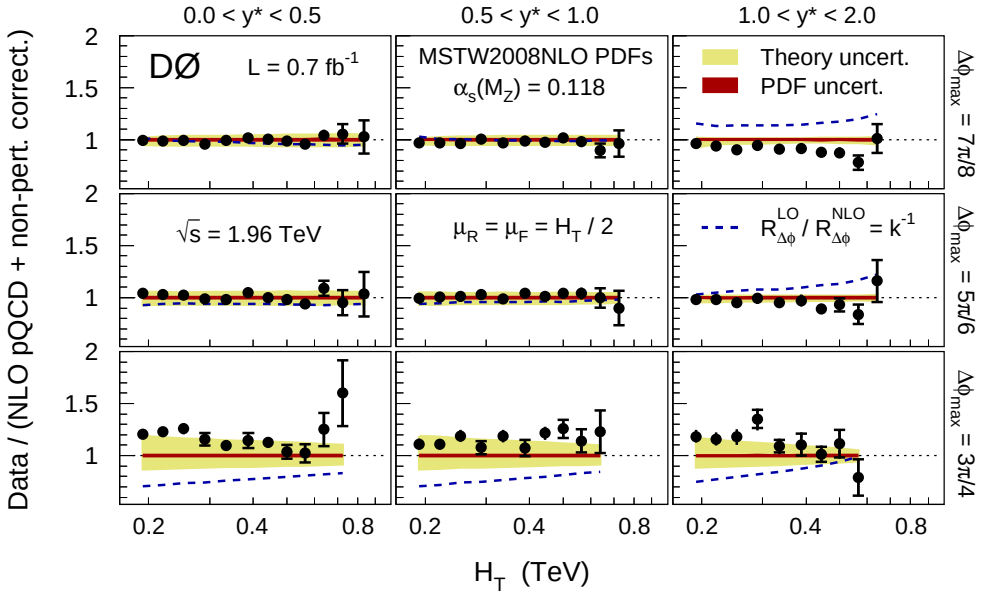

FIG. 3: (Color online.) Ratios of the results of $R_{\Delta\phi}$ and the theoretical predictions obtained for MSTW2008NLO PDFs and $\alpha_s(M_Z) = 0.118$. The ratios are shown as a function of H_T in different regions of y^* and for different $\Delta\phi_{\rm max}$. The inner error bars indicate the statistical uncertainties, and the outer error bars the statistical and systematic uncertainties summed in quadrature. The theoretical uncertainty is the PDF and scale uncertainty summed in quadrature. Also shown is the ratio of the LO and NLO pQCD predictions which is the inverse of the NLO k-factor.

by the uncertainties of the pQCD calculations due to the μ_R and μ_F dependencies. These are computed as the relative changes of the results due to independent variations of both scales between $\mu_0/2$ and $2\mu_0$, with the restriction of $0.5 \leq \mu_R/\mu_F \leq 2.0$. The uncertainties from the scale dependence are 4–6% for $\Delta\phi_{\rm max} = 7\pi/8$ and $5\pi/6$, and 6–20% for $\Delta\phi_{\rm max} = 3\pi/4$, decreasing with H_T. In addition to the scale dependence, the NLO k-factors provide additional information on the convergence of the perturbative expansion, and therefore on the possible size of missing higher order contributions. The NLO k-factors are computed as the ratio of the NLO and the LO predictions for $R_{\Delta\phi}$ ($k = R^{\rm NLO}_{\Delta\phi}/R^{\rm LO}_{\Delta\phi}$). Figure 3 shows the inverse of the NLO k-factors and their dependence on y^* and $\Delta\phi_{\rm max}$.

Ratios of data and the theoretical predictions are displayed in Fig. 3 as a function of H_T in all regions of y^* and $\Delta\phi_{\rm max}$. To quantify the agreement, χ^2 values are determined that compare data and theory, taking into account the correlations between all uncertainties. The χ^2 definition is the same that was used in our recent α_s determinations [12, 34]. Table IV displays the χ^2 values for all H_T bins within each of the nine kinematic regions in y^* and $\Delta\phi_{\rm max}$. The results are shown for three different choices of μ_R and μ_F, including the central choice $\mu_R = \mu_F = H_T/2$ and the combined lower and upper variations, $H_T/4$ and H_T. The following discussion distinguishes between the three different kinematic regions, which are given by $\Delta\phi_{\rm max} = 3\pi/4$, by $y^* > 1$, and by $y^* < 1$ with $\Delta\phi_{\rm max} = 7\pi/8$ or $5\pi/6$.

The region of large azimuthal decorrelations, $\Delta\phi_{\rm max} = 3\pi/4$, is challenging for the theoretical predictions, since it receives large contributions from four-jet final states. These are only modeled at LO by the $\mathcal{O}(\alpha_s^4)$ calculation for the numerator of $R_{\Delta\phi}$, which causes the large NLO k-factors (up to 1.5) and the large scale dependence (up to 21%), seen in Fig. 3. In this kinematic region, the central theoretical predictions are consistently below the data (often by 15–25%). Within the large scale uncertainty, however, they agree with the data, as the χ^2 values for the lower scale choice $H_T/4$ are all consistent with the expectations based on the number of degrees of freedom ($N_{\rm dof}$, which corresponds here to the number of data points), of $\chi^2 = N_{\rm dof} \pm \sqrt{2\,N_{\rm dof}}$.

In the kinematic region $y^* > 1$, the theoretical predictions exhibit a different H_T dependence as compared to lower y^*, as seen in Fig. 1. While at lower y^* the predicted H_T dependence of the $R_{\Delta\phi}$ distributions is monotonically decreasing, the H_T distributions for $y^* > 1$ have a local minimum around ≈ 0.5 TeV above which $R_{\Delta\phi}$ increases. For $\Delta\phi_{\rm max} = 5\pi/6$, the theoretical predictions give an adequate description of the data. For $\Delta\phi_{\rm max} = 7\pi/8$, however, the predicted H_T dependence differs from that of the measured $R_{\Delta\phi}$ distribution, as quantified by the large χ^2 regardless of the scale choice. This is the only kinematic region in ($\Delta\phi_{\rm max}$, y^*) for which the NLO k-factor is consistently below unity (0.89–0.81) over the entire H_T range. This may indicate a poor convergence of the perturbative expansion.

The perturbative expansion works best in the kine-

TABLE I: The results for $R_{\Delta\phi}$ with their relative uncertainties for $\Delta\phi_{\rm max} = 7\pi/8$.

H_T (GeV)	y^*	$R_{\Delta\phi}$	Stat. uncert. (percent)	Syst. uncert. (percent)	
180–205	0.0–0.5	2.216×10^{-1}	±0.9	+2.8	−3.0
205–235	0.0–0.5	2.116×10^{-1}	±1.1	+2.6	−2.6
235–270	0.0–0.5	2.000×10^{-1}	±1.5	+2.5	−2.3
270–310	0.0–0.5	1.811×10^{-1}	±2.2	+2.2	−2.2
310–360	0.0–0.5	1.731×10^{-1}	±1.5	+2.0	−2.1
360–415	0.0–0.5	1.641×10^{-1}	±2.4	+1.9	−1.9
415–470	0.0–0.5	1.491×10^{-1}	±1.5	+1.9	−1.9
470–530	0.0–0.5	1.359×10^{-1}	±2.4	+1.9	−1.9
530–600	0.0–0.5	1.206×10^{-1}	±3.2	+2.0	−2.0
600–680	0.0–0.5	1.204×10^{-1}	±5.0	+2.2	−2.1
680–770	0.0–0.5	1.114×10^{-1}	±8.8	+2.4	−2.3
770–900	0.0–0.5	9.699×10^{-2}	±15.4	+2.5	−2.3
180–205	0.5–1.0	2.311×10^{-1}	±0.9	+2.9	−3.3
205–235	0.5–1.0	2.252×10^{-1}	±1.2	+2.8	−2.9
235–270	0.5–1.0	2.115×10^{-1}	±1.6	+2.6	−2.5
270–310	0.5–1.0	2.085×10^{-1}	±2.3	+2.4	−2.3
310–360	0.5–1.0	1.888×10^{-1}	±1.7	+2.2	−2.2
360–415	0.5–1.0	1.808×10^{-1}	±2.8	+2.1	−2.1
415–470	0.5–1.0	1.686×10^{-1}	±1.8	+2.1	−2.0
470–530	0.5–1.0	1.662×10^{-1}	±2.8	+2.1	−2.1
530–600	0.5–1.0	1.517×10^{-1}	±3.9	+2.2	−2.1
600–680	0.5–1.0	1.318×10^{-1}	±7.3	+2.4	−2.1
680–770	0.5–1.0	1.356×10^{-1}	±13.0	+2.5	−2.2
180–205	1.0–2.0	2.934×10^{-1}	±1.0	+3.8	−4.4
205–235	1.0–2.0	2.850×10^{-1}	±1.3	+3.7	−4.0
235–270	1.0–2.0	2.634×10^{-1}	±2.0	+3.6	−3.4
270–310	1.0–2.0	2.667×10^{-1}	±2.9	+3.3	−2.9
310–360	1.0–2.0	2.502×10^{-1}	±2.3	+3.1	−2.6
360–415	1.0–2.0	2.468×10^{-1}	±4.0	+3.1	−2.6
415–470	1.0–2.0	2.317×10^{-1}	±3.0	+3.1	−2.7
470–530	1.0–2.0	2.320×10^{-1}	±5.2	+3.0	−2.7
530–600	1.0–2.0	2.116×10^{-1}	±8.6	+2.8	−2.8
600–680	1.0–2.0	2.875×10^{-1}	±13.7	+2.7	−2.8

TABLE II: The results for $R_{\Delta\phi}$ with their relative uncertainties for $\Delta\phi_{\rm max} = 5\pi/6$.

H_T (GeV)	y^*	$R_{\Delta\phi}$	Stat. uncert. (percent)	Syst. uncert. (percent)	
180–205	0.0–0.5	1.439×10^{-1}	±1.1	+2.8	−2.6
205–235	0.0–0.5	1.325×10^{-1}	±1.4	+2.5	−2.5
235–270	0.0–0.5	1.223×10^{-1}	±2.0	+2.3	−2.3
270–310	0.0–0.5	1.097×10^{-1}	±3.0	+2.1	−2.1
310–360	0.0–0.5	1.007×10^{-1}	±2.1	+2.0	−2.0
360–415	0.0–0.5	9.851×10^{-2}	±3.3	+2.0	−1.9
415–470	0.0–0.5	8.635×10^{-2}	±2.1	+2.0	−2.0
470–530	0.0–0.5	7.821×10^{-2}	±3.2	+2.0	−2.0
530–600	0.0–0.5	6.832×10^{-2}	±4.3	+2.1	−2.1
600–680	0.0–0.5	7.262×10^{-2}	±6.6	+2.2	−2.3
680–770	0.0–0.5	5.760×10^{-2}	±12.5	+2.3	−2.4
770–900	0.0–0.5	5.600×10^{-2}	±20.7	+2.6	−2.7
180–205	0.5–1.0	1.463×10^{-1}	±1.4	+3.2	−2.9
205–235	0.5–1.0	1.396×10^{-1}	±1.6	+2.6	−2.6
235–270	0.5–1.0	1.317×10^{-1}	±2.2	+2.4	−2.5
270–310	0.5–1.0	1.263×10^{-1}	±3.1	+2.2	−2.3
310–360	0.5–1.0	1.139×10^{-1}	±2.3	+2.2	−2.2
360–415	0.5–1.0	1.117×10^{-1}	±3.6	+2.1	−2.1
415–470	0.5–1.0	1.016×10^{-1}	±2.4	+2.1	−2.1
470–530	0.5–1.0	9.993×10^{-2}	±3.8	+2.1	−2.1
530–600	0.5–1.0	9.414×10^{-2}	±5.1	+2.2	−2.2
600–680	0.5–1.0	8.566×10^{-2}	±9.2	+2.2	−2.3
680–770	0.5–1.0	7.369×10^{-2}	±18.2	+2.3	−2.5
180–205	1.0–2.0	1.926×10^{-1}	±1.3	+4.0	−3.5
205–235	1.0–2.0	1.840×10^{-1}	±1.8	+3.7	−3.5
235–270	1.0–2.0	1.709×10^{-1}	±2.6	+3.3	−3.4
270–310	1.0–2.0	1.716×10^{-1}	±3.9	+3.0	−3.2
310–360	1.0–2.0	1.611×10^{-1}	±3.0	+3.0	−3.1
360–415	1.0–2.0	1.600×10^{-1}	±5.2	+3.0	−3.1
415–470	1.0–2.0	1.436×10^{-1}	±4.0	+3.0	−3.0
470–530	1.0–2.0	1.518×10^{-1}	±6.7	+2.9	−3.1
530–600	1.0–2.0	1.391×10^{-1}	±11.0	+2.8	−3.1
600–680	1.0–2.0	2.034×10^{-1}	±17.2	+2.9	−3.2

matic regions of $0 < y^* < 0.5$ and $0.5 < y^* < 1.0$, where the scale dependence is small (< 6%) and the NLO k-factors are above unity but small ($1.00 < k < 1.06$). In all of those regions, the theoretical predictions give a good description of the data.

In summary, the first measurement of the combined rapidity and p_T dependence of dijet azimuthal decorrelations is presented. The measurement is based on the recently proposed quantity $R_{\Delta\phi}$, which probes dijet azimuthal decorrelations in a novel way. It is measured in $p\bar{p}$ collisions at $\sqrt{s} = 1.96\,\text{TeV}$ as a function of the total transverse momentum H_T, the rapidity y^*, and the parameter $\Delta\phi_{\rm max}$. For all values of $\Delta\phi_{\rm max}$ and at fixed H_T, dijet azimuthal decorrelations increase with y^*, while they decrease with H_T over most of the H_T range at fixed y^*. Predictions of NLO pQCD, corrected for nonperturbative effects, give a good description of the data, except in the kinematic region of large dijet rapidity intervals $y^* > 1$ and small decorrelations $\Delta\phi_{\rm max} = 7\pi/8$.

We thank the staffs at Fermilab and collaborating institutions, and acknowledge support from the DOE and NSF (USA); CEA and CNRS/IN2P3 (France); MON, NRC KI and RFBR (Russia); CNPq, FAPERJ, FAPESP and FUNDUNESP (Brazil); DAE and DST (India); Colciencias (Colombia); CONACyT (Mexico); NRF (Korea); FOM (The Netherlands); STFC and the Royal Society (United Kingdom); MSMT and GACR (Czech Republic); BMBF and DFG (Germany); SFI (Ireland); The Swedish Research Council (Sweden); and CAS and CNSF (China).

[1] Rapidity y is related to the polar scattering angle θ with respect to the proton beam direction by $y = \frac{1}{2}\ln[(1+\beta\cos\theta)/(1-\beta\cos\theta)]$, where β is defined as the ratio of the magnitude of momentum and energy, $\beta = |\vec{p}|/E$. In $2 \to 2$ processes, the variable y^* corre-

TABLE III: The results for $R_{\Delta\phi}$ with their relative uncertainties for $\Delta\phi_{\rm max} = 3\pi/4$.

H_T (GeV)	y^*	$R_{\Delta\phi}$	Stat. uncert. (percent)	Syst. uncert. (percent)	
180–205	0.0–0.5	4.659×10^{-2}	±2.0	$+2.8$	-2.7
205–235	0.0–0.5	4.339×10^{-2}	±2.6	$+2.7$	-2.5
235–270	0.0–0.5	4.055×10^{-2}	±3.5	$+2.3$	-2.2
270–310	0.0–0.5	3.405×10^{-2}	±5.4	$+2.2$	-2.2
310–360	0.0–0.5	2.913×10^{-2}	±4.0	$+2.2$	-2.2
360–415	0.0–0.5	2.733×10^{-2}	±6.2	$+2.2$	-2.3
415–470	0.0–0.5	2.419×10^{-2}	±4.0	$+2.2$	-2.4
470–530	0.0–0.5	2.008×10^{-2}	±6.3	$+2.1$	-2.6
530–600	0.0–0.5	1.780×10^{-2}	±8.4	$+2.3$	-2.8
600–680	0.0–0.5	1.953×10^{-2}	±12.6	$+2.7$	-3.1
680–770	0.0–0.5	2.241×10^{-2}	±19.8	$+3.8$	-3.5
180–205	0.5–1.0	4.620×10^{-2}	±2.6	$+3.9$	-3.9
205–235	0.5–1.0	4.261×10^{-2}	±3.0	$+3.2$	-3.1
235–270	0.5–1.0	4.152×10^{-2}	±3.9	$+2.7$	-2.7
270–310	0.5–1.0	3.510×10^{-2}	±6.0	$+2.6$	-2.8
310–360	0.5–1.0	3.578×10^{-2}	±4.1	$+2.6$	-2.9
360–415	0.5–1.0	2.962×10^{-2}	±7.1	$+2.7$	-2.9
415–470	0.5–1.0	3.107×10^{-2}	±4.3	$+2.7$	-2.9
470–530	0.5–1.0	2.984×10^{-2}	±6.9	$+2.6$	-2.9
530–600	0.5–1.0	2.532×10^{-2}	±9.8	$+2.6$	-3.2
600–680	0.5–1.0	2.587×10^{-2}	±16.7	$+3.1$	-3.4
180–205	1.0–2.0	6.873×10^{-2}	±2.5	$+4.8$	-3.9
205–235	1.0–2.0	6.402×10^{-2}	±3.3	$+4.5$	-4.1
235–270	1.0–2.0	6.169×10^{-2}	±4.6	$+4.3$	-4.5
270–310	1.0–2.0	6.741×10^{-2}	±6.4	$+4.1$	-4.8
310–360	1.0–2.0	5.218×10^{-2}	±5.5	$+4.2$	-4.7
360–415	1.0–2.0	5.049×10^{-2}	±9.5	$+4.3$	-4.5
415–470	1.0–2.0	4.505×10^{-2}	±7.2	$+4.3$	-4.4
470–530	1.0–2.0	4.899×10^{-2}	±11.9	$+4.1$	-4.7
530–600	1.0–2.0	3.504×10^{-2}	±22.0	$+3.6$	-5.6

sponds to the absolute value of the rapidities of the two jets in the dijet center-of-mass frame frame (see Ref. [5]).

[2] V. M. Abazov *et al.*, D0 Collaboration, Phys. Rev. Lett. **94**, 221801 (2005).

[3] V. Khachatryan *et al.*, CMS Collaboration, Phys. Rev. Lett. **106**, 122003 (2011).

[4] G. Aad *et al.*, ATLAS Collaboration, Phys. Rev. Lett. **106**, 172002 (2011).

[5] M. Wobisch *et al.*, submitted to J. High Energy Phys., arXiv:1211.6773 [hep-ph].

[6] G. C. Blazey *et al.*, in: U. Baur, R. K. Ellis, and D. Zeppenfeld (Eds.), *Proceedings of the Workshop: QCD and Weak Boson Physics in Run II*, Fermilab-Pub-00/297 (2000).

[7] C. Buttar *et al.*, in: G. Belanger *et al.* (Eds.), *Les Houches 2007, Physics at TeV colliders*, arXiv:0803.0678 [hep-ph], section 9.

[8] V. M. Abazov *et al.*, D0 Collaboration, Nucl. Instrum. Methods Phys. Res. A **565**, 463 (2006).

[9] V. M. Abazov *et al.*, D0 Collaboration, Phys. Rev. Lett. **103**, 191803 (2009).

[10] V. M. Abazov *et al.*, D0 Collaboration, Phys. Lett. B **693**, 531 (2010).

[11] V. M. Abazov *et al.*, D0 Collaboration, Phys. Lett. B **704**, 434 (2011).

[12] V. M. Abazov *et al.*, D0 Collaboration, Phys. Lett. B **718**, 56 (2012).

[13] V. M. Abazov *et al.*, D0 Collaboration, Submitted to Phys. Lett. B, arXiv:1209.1140 [hep-ex].

[14] V. M. Abazov *et al.*, D0 Collaboration, Phys. Rev. Lett. **101**, 062001 (2008).

[15] V. M. Abazov *et al.*, D0 Collaboration, Phys. Rev. D **85**, 052006 (2012).

[16] T. Sjöstrand *et al.*, Comput. Phys. Commun. **135**, 238 (2001).

[17] R. Brun and F. Carminati, CERN Program Library Long Writeup W5013, 1993.

[18] T. Gleisberg *et al.*, J. High Energy Phys. **02**, 007 (2009).

[19] A. D. Martin *et al.*, Eur. Phys. J. C **63**, 189 (2009).

[20] P. M. Nadolsky *et al.*, Phys. Rev. D **78**, 013004 (2008).

[21] M. G. Albrow *et al.*, TeV4LHC QCD Working Group, hep-ph/0610012.

[22] Supplementary material is available in the online version of this Letter available at doi:10.1016/j.physletb.YYYY.MM.AAA.

[23] G. Brandt in: M. Diehl, J. Haller, T. Schörner-Sadenius and G. Steinbrück (Eds.), in *5th Conference: Physics at the LHC 2010*, DESY-PROC-2010-01 (2010).

[24] G. Corcella *et al.*, J. High Energy Phys. **01**, 010 (2001).

[25] G. Corcella *et al.*, hep-ph/0210213.

[26] T. Kluge, K. Rabbertz, and M. Wobisch, hep-ph/0609285.

[27] M. Wobisch *et al.*, fastNLO Collaboration, arXiv:1109.1310 [hep-ph].

[28] Z. Nagy, Phys. Rev. D **68**, 094002 (2003).

[29] Z. Nagy, Phys. Rev. Lett. **88**, 122003 (2002).

[30] W. A. Bardeen, A. J. Buras, D. W. Duke, and T. Muta, Phys. Rev. D **18**, 3998 (1978).

[31] J. Beringer *et al.* (Particle Data Group), Phys. Rev. D **86**, 010001 (2012).

[32] H. L. Lai *et al.*, Phys. Rev. D **82**, 074024 (2010).

[33] R. D. Ball *et al.*, Nucl. Phys. B **849**, 296 (2011).

[34] V. M. Abazov *et al.*, D0 Collaboration, Phys. Rev. D **80**, 111107 (2009).

TABLE IV: The χ^2 values between data and theory for MSTW2008PDFs and $\alpha_s(M_Z) = 0.118$ and for different choices of μ_R and μ_F. The results are shown for each of the nine kinematic regions, defined by the y^* and $\Delta\phi_{\rm max}$ requirements, combining all H_T bins inside those regions.

y^* range	$\Delta\phi_{\rm max}$	$N_{\rm dof}$	χ^2 for $\mu_R = \mu_F =$ $H_T/4$	$H_T/2$	H_T
0.0–0.5	$7\pi/8$	12	15.1	7.1	12.7
0.0–0.5	$5\pi/6$	12	15.7	10.9	20.9
0.0–0.5	$3\pi/4$	11	13.1	44.2	104.5
0.5–1.0	$7\pi/8$	11	11.8	6.9	8.6
0.5–1.0	$5\pi/6$	11	5.6	4.0	12.6
0.5–1.0	$3\pi/4$	10	15.4	26.9	60.2
1.0–2.0	$7\pi/8$	10	29.7	24.4	19.8
1.0–2.0	$5\pi/6$	10	9.3	10.8	10.7
1.0–2.0	$3\pi/4$	9	10.3	23.1	45.5